

1 Sorption Phenomena In Transient Vapor Intrusion
2 Scenarios

3 Jonathan G. V. Ström^a, Shuai Xie^a, Eric M. Suuberg^a

4 *These authors contributed equally to this work*

5 ^a*Brown University, School of Engineering, Providence, RI, USA*

6 **Abstract**

Abstract here

7 *Keywords:* Vapor intrusion, Temporal variability, Sorption, Attenuation
8 factor

9 **1. Introduction**

10 Many vapor intrusion (VI) contaminants has the capacity to sorb onto soil
11 and various common indoor materials, but the role and more importantly,
12 the consequences of these sorption processes in VI are poorly understood[1,
13 2, 3]. The migration of contaminant vapors from its source into the VI
14 affected building and potential indoor sources is usually the prime concern
15 in VI investigations. Rarely is the sorbed contaminant vapors in the soil
16 or indoor considered in an investigation, but these may potentially act as a
17 capacitor, storing and releasing contaminant vapors in response to a change in
18 contaminant concentration. Consequently, contaminant vapors may be much
19 more persistent at a site that has undergone remediation, potentially reducing
20 the effectiveness of mitigation systems, or impeding site investigations.

21 It is well recognized that building materials has the capacity to sorb pol-
22 lutants. The sorptive capacity of various volatile organic compounds (VOCs)
23 of concern in VI have been tested on a variety of building materials, such as
24 density board[4], gypsum wallboard[5], and plywood and carpets[6]. How-
25 ever, most of these studies used relative high contaminant concentrations,
26 usually around mg/m³[4] or even higher. This is several magnitudes higher
27 than the concentrations relevant in VI and due to the non-linear nature of
28 sorption with respect to concentration, sorption studies at lower concentra-
29 tion are needed.

30 Most of the VOC sorption studies have also focused on the interaction be-
31 tween building materials and formaldehyde[5], toluene, and decane[6]. How-
32 ever, one of the contaminants of greatest concern in VI - trichloroethylene
33 (TCE), has not received likewise attention. This is despite the fact that sorb-
34 ing TCE (and other VOCs) on activated carbon is extensively used to treat
35 indoor air contaminant and their use with passive sorption tube samplers[7].

36 Over the years many VI sites have been investigated for their potential
37 exposure risk. Two well-known examples of these are the studies of a house
38 in Layton, Utah and one in Indianapolis, Indiana. Both of these sites were
39 outfitted with a wide variety of instrumentation to measure various metrics
40 such as contaminant concentration in interior, soil, and groundwater, as well
41 as things like pressure, temperature, or weather. These studies yielded some
42 of the richest VI datasets available and gave invaluable insights, in particular
43 in the application of CPM[8] and sub-slab depressurization (SSD) mitigation
44 systems[9, 10]. However, neither of these studies considered the role of sorp-
45 tion had at these sites.

46 The potential impact of sorption could perhaps be most significant in
47 the application of the controlled pressure method (CPM) and various mit-
48 igation schemes. The controlled pressure method is the forced over- and
49 depressurization of a building to max- and minimize the contaminant entry
50 into the building. This can help the investigator ascertain the worst-case VI
51 scenario and help identify potential indoor contaminant sources[11, 8]. How-
52 ever, if the building indoor materials has a large sorptive capacities, then de-
53 and sorption processes may significantly affect the indoor air contaminant
54 concentration. Likewise, a significant amount of sorbed material may be re-
55 leased from the interior over an unknown period of time after mitigating the
56 contaminant intrusion at a site[1, 2].

57 In the past VI models have been used to gain insight into VI when no
58 field or experimental data has been available. Previously examples of VI
59 modeling studies are the role of rainfall in VI[12], or drivers of temporal
60 variability in some of the aforementioned sites[13]. However, while many VI
61 models include a sorption term in the governing equation for contaminant
62 transport in soils, none have explored the role of sorption in VI in a transient
63 simulation. The reason for this is two-fold. First, there has been a general
64 lack of interest in sorption and VI thus far. Secondly, the vast majority of VI
65 modeling efforts and studies has focused on steady-state analyses of VI, and
66 sorption only affects soil contaminant transport in time-dependent scenarios.

67 To bridge this knowledge gap we will begin to explore the role of sorp-

tion in VI through a combined effort of experimental and simulation work. Sorption data of TCE on various cinderblock, drywall, wood, paper, carpet, and Appling soil will be measured in a fixed bed sorption experiment. These sorption data will be used to generate kinetic sorption parameters to be used in our three-dimensional finite element VI model. For this purpose we will consider a prototypical VI scenario where a free-standing house with a basement is overlying a homogenously contaminated groundwater source. Using this model we will investigate how the dynamic contaminant transport is affected in general by sorption, how indoor sorption materials affect indoor air concentration as the building's pressurization fluctuates and how indoor air concentration are affected by indoor materials following successful mitigation of the structure.

2. Methods

2.1. Experimental Setup

To study the dynamic sorption of TCE onto the selected building materials, we use a two-step process - one for sorption and one for desorption. A graphic representation of this system is shown in Figure 1.

In the sorption process a 7.5 by 1.27 cm stainless steel column is filled with material. (Before filling the column, the materials had to be ground-up using a coffee grinder, except soil. We use 2.0 g of drywall, and 1.0 g of the other materials.) Using flow controllers, TCE is diluted in nitrogen gas to 1.12 ppb_v and flowed through the column at a rate of 60 mL per minute, for a pre-selected time period. After the material has sorbed for the selected time, the column is detached and attached to the desorption system.

In the desorption system, the column is heated to 100 °C and pure nitrogen gas is flowed through the previous outlet side of the column - carrying the desorbed contaminant with it. The now contaminated nitrogen gas is then passed through a long circular pipe, allowing the gas to cool to room temperature, and flowing into a carbon-filled stainless steel sorption column. The sorption column is then desorbed into a gas-chromatograph fitted with a electron capture device according to the EPA TO-17 standard.

2.2. Numerical Model

To investigate the role of sorption in VI, we consider VI impacted house with a 10 by 10 m footprint, with the foundation bottom located 1 m below ground surface (bgs). The sole contaminant source is an uniformly TCE

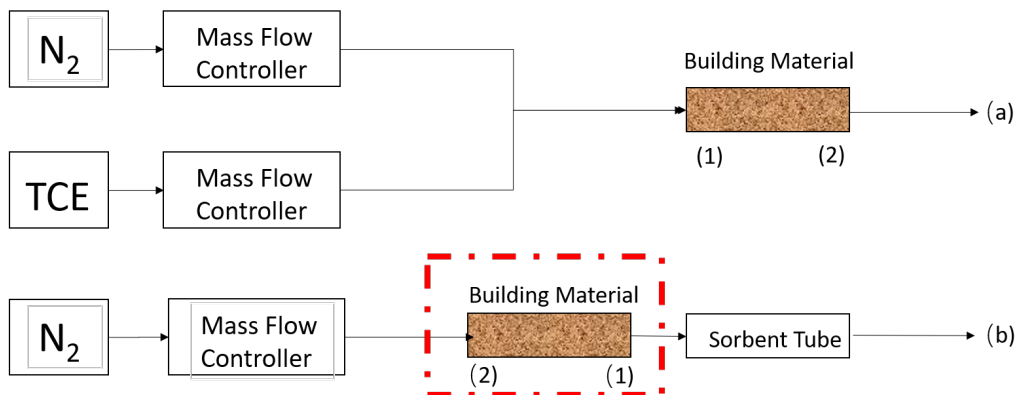


Figure 1: Schematic of experimental setup.

Figure 2: The vapor intrusion model. Not yet done.

103 contaminated groundwater located 4 bgs, and the soil surrounding the house
 104 is assumed to homogenous and of a singular type. All contaminant vapors
 105 are assumed to enter the house through breaches in the foundation, modeled
 106 as a 1 cm wide crack that runs along the perimeter of the house. Finally
 107 we assume that sorption processes can occur both in the soil matrix and
 108 in the indoor environment (on various indoor materials). Figure 2 shows a
 109 schematic of this model.

110 Modeling this scenario requires us to simulate a couple of physics, many
 111 of which depend and interact with each other. The soil contains a variable
 112 moisture content and is modeled using van Genuchten's retention model[14],
 113 which determines the effective permeability of the soil matrix and the con-
 114 taminant effective diffusivity. Darcy's Law models the gas velocity in the soil
 115 matrix, which is used to determine the advective mass transport. Contami-
 116 nant mass transport is assumed to occur through advection and diffusion, and
 117 distributed between gas, water, and sorbed onto solid phases. The indoor air
 118 space is modeled using as a continuously stirred tank reactor (CSTR), where
 119 the reaction term determines the sorption onto/from the indoor materials.
 120 It is important to note that the indoor environment is implicitly modeled,
 121 but instead only given by the CSTR equation; the soil domain is explicitly
 122 modeled.

123 2.2.1. Vadose Zone Moisture Content

124 Since the contaminant transport occurs through three-phased the vadose
 125 zone, it is important that we correctly account for soil moisture content and
 126 its effect on advective and diffusive transport. In this modeled scenario, we
 127 assume that the soil moisture is at steady-state and does not change, and
 128 thus the soil moisture content is given by the retention model developed by
 129 van Genuchten[14].

The van Genuchten retention model gives the soil water saturation as a function of elevation above groundwater. In turn this gives the water and gas filled porosities, and the relative permeability of the soil matrix.

$$\text{Se} = \begin{cases} \frac{1}{(1+\alpha z^n)^m} & z < 0 \\ 1 & z \geq 0 \end{cases} \quad (1)$$

$$\theta_w = \begin{cases} \theta_r + \text{Se}(\theta_s - \theta_r) & z < 0 \\ \theta_s & z \geq 0 \end{cases} \quad (2)$$

$$k_r = \begin{cases} \text{Se}^l [1 - (1 - \text{Se}^{\frac{1}{m}})]^2 & z < 0 \\ 0 & z \geq 0 \end{cases} \quad (3)$$

130 Se is the saturation, and ranges from 0 to 1, which represent completely un-
 131 to fully saturated; z is the elevation above the groundwater in meters; θ_r ,
 132 θ_s , θ_w , and θ_g are the residual moisture content, saturated porosity (or just
 133 porosity), and water and air filled porosities respectively. All units are in
 134 volume of phase divided by the volume of soil; k_r is the relative permeability
 135 of water, which modifies the saturated permeability. This too ranges from 0
 136 to 1, indicating completely im- and permeable respectively. $1 - k_r$ gives the
 137 relative permeability of air.

138 2.2.2. Gas Flow In The Vadose Zone

139 The gas flow in the vadose zone is governed by a modified version of
 140 Darcy's Law. Originally, Darcy's Law was developed to describe flow in
 141 saturated porous media, but since we're interested in flow in unsaturated
 142 media, modification is necessary. An effective permeability that depends
 143 on the relative permeability from van Genuchten is introduced to allow for
 144 correct flow profiles in unsaturated porous media.

145 The vapor flow continuity governing equation is given by

$$\frac{\partial}{\partial t}(\rho\theta_s) + \nabla \cdot \rho \left(- \frac{(1 - k_r)\kappa}{\mu} \nabla p \right) = 0 \quad (4)$$

146 Here ρ is the fluid density; ∇ is the del operator; κ is the saturated per-
 147 meability; μ is the fluid viscosity; and p is the fluid pressure. We assume
 148 that the contaminant vapors are so dilute that the gas flow properties can
 149 be taken to be those of air, and specifically at 20 °C and all the transport
 150 properties may be found in Table 1.

Boundary Conditions. To solve (4) we assign the atmosphere boundary (see Figure 2) to be at reference pressure and act as a gauge, i.e. zero pressure. The foundation crack boundary is assigned the indoor-outdoor pressure difference value. Remaining boundaries are no-flow boundary conditions.

$$\begin{array}{ll} \text{Atmosphere} & p = 0 \text{ (Pa)} \end{array} \quad (5)$$

$$\begin{array}{ll} \text{Foundation crack} & p = p_{\text{in/out}} \text{ (Pa)} \end{array} \quad (6)$$

$$\begin{array}{ll} \text{All other} & -\vec{n} \cdot \rho_{\text{air}} \vec{u} = 0 \text{ (kg/(m}^2 \cdot \text{s))} \end{array} \quad (7)$$

151 Here \vec{n} and \vec{u} are the boundary normal and gas velocity vectors.

152 *Initial Conditions.* For steady-state problems, the initial conditions do not
 153 influence the solution, but by necessity simply set to zero for the entire
 154 domain. Transient simulations however, use the initial conditions that are
 155 given by the steady-state solution.

156 2.2.3. Mass Transport In The Vadose Zone

157 Contaminants in the vadose zone exist in three phases - gaseous, solved in
 158 water, and sorbed onto soil particles. While there are three distinct phases,
 159 the water and gas phases are related via Henry's Law (8).

$$c_g = K_H c_w \quad (8)$$

160 Where c_g and c_w are the gas and water phase concentrations respectively in
 161 mol/m³; K_H is the dimensionless Henry's Law constant.

162 In this work, we consider sorption between the soil and vapor phases, as
 163 a function of the water contaminant concentration, through linear sorption
 164 (9).

$$c_s = K_{\text{ads}} \rho_b c_g = K_{\text{ads}} \frac{\rho}{1 - \theta_t} K_H c_w \quad (9)$$

165 Here the c_s is the solid phase concentration in mol/kg; ρ_b is the bulk density
 166 of the soil kg/m³, which is given by the density ρ and the total soil porosity
 167 θ_t ; K_{ads} is the sorption isotherm in m³/kg. Using Henry's Law and the linear

168 isotherm we can express the total contaminant concentration in terms of the
 169 water contaminant concentration.

170 Mass transport in the vadose zone is governed by diffusion and advection
 171 and is given by (10).

$$R \frac{\partial c}{\partial t} = \nabla \cdot [D_{\text{eff}} \nabla c] - K_H \vec{u} \cdot \nabla c \quad (10)$$

172 The first term in (10) gives the change in contaminant water concentration
 173 with respect to time, modified by the *retardation factor*, R , which is discussed
 174 below; The second is the effective diffusive flux which is modified by the
 175 effective diffusion coefficient D_{eff} which is also discussed below. The third is
 176 the advective flux where \vec{u} is the soil-gas velocity from Darcy's Law, which
 177 when multiplied with K_H gives the gas phase concentration advective flux.

178 *Contaminant entry into the building.* The contaminant enters the building
 179 through a combination of advection and diffusive fluxes and is given by (11).

$$j_{ck} = \begin{cases} u_{ck} c_g - \frac{D_{\text{air}}}{L_{\text{slab}}} (c_{in} - c_g) & u_{ck} \geq 0 \\ u_{ck} c_{in} - \frac{D_{\text{air}}}{L_{\text{slab}}} (c_{in} - c_g) & u_{ck} < 0 \end{cases} \quad (11)$$

180 Here the j_{ck} is the molar contaminant flux into the building in $\text{mol}/(\text{m}^2 \cdot \text{s})$;
 181 D_{air} is the contaminant diffusion coefficient in pure air in m^2/s ; L_{slab} is the
 182 thickness of the foundation slab in m. The flux expression changes if there
 183 is a bulk flow into the building, i.e. $u_{ck} \geq 0$, or out of the building.

184 *Retardation factor.* As the contaminants are transported through the vadose
 185 zone, the partitioning between the various phases increases the contaminant
 186 residency time, retarding the transport of contaminants. This effect is rep-
 187 resented by R which is the retardation factor (12).

$$R = \theta_w + \theta_g K_H + \rho_b K_H K_{\text{ads}} \quad (12)$$

Here θ_w , θ_g are the water and gas filled soil porosities; K_{ads} is the solid-gas
 phase sorption isotherm in m^3/kg . The diffusive and advective transport
 retardation is proportional to the inverse of R .

$$D_{\text{retarded}} = \frac{D_{\text{eff}}}{R} \quad (13)$$

$$\vec{u}_{\text{retarded}} = \frac{\vec{u}}{R} \quad (14)$$

188 It should be noted that the soil-gas velocity, \vec{u} , is not retarded in of itself,
 189 but rather just the contaminant being transported through advection, giving
 190 a effective bulk velocity.

191 *Effective diffusivity.* The effective diffusivity in the vadose zone varies with
 192 the soil moisture content, from being close to that in water when fully sat-
 193 urated and vice versa. Millington-Quirk developed (15) which describes the
 194 effective diffusivity in variably saturated porous media.

$$D_{\text{eff}} = D_{\text{water}} \frac{\theta_w^{\frac{7}{3}}}{\theta_t^2} + \frac{D_{\text{air}}}{K_H} \frac{\theta_g^{\frac{7}{3}}}{\theta_t^2} \quad (15)$$

195 Where the porosity fractions are the water and gas phase tortuosity terms;
 196 D_{air} and D_{water} are the contaminant diffusion coefficient in air and water
 197 respectively in m^2/s .

Boundary Conditions. A few boundary conditions are required to solve (10).
 In this model, the sole contaminant source is assumed to be the homogenously
 contaminated groundwater, which we assume to have a fixed concentration.
 The atmosphere acts as a contaminant sink, and any contaminant that makes
 it to this boundary is infinitely diluted, thus this is simply a zero concentra-
 tion boundary condition. Contaminants leave the soil domain and enter the
 building through a combination of advective and diffusive gas phase trans-
 port. The last boundary condition is applied to all other boundaries and is
 a no-flow boundary.

$$\text{Groundwater} \quad c_w = 0 \text{ (mol/m}^3\text{)} \quad (16)$$

$$\text{Atmosphere} \quad c_w = c_{gw} \text{ (mol/m}^3\text{)} \quad (17)$$

$$\text{Foundation crack} \quad -\vec{n} \cdot \vec{N} = -\frac{j_{ck}}{K_H} \text{ (mol/(m}^2 \cdot \text{s))} \quad (18)$$

$$\text{All other} \quad -\vec{n} \cdot \vec{N} = 0 \text{ (mol/(m}^2 \cdot \text{s))} \quad (19)$$

198 $\vec{n} \cdot \vec{N}$ is the dot product between the boundary normal vector and the contam-
 199 inant flux; j_{ck} is the contaminant vapor flux into the building. We assume
 200 that only contaminants in the gas phase enter the building, and dividing j_{ck}
 201 by K_H we get proper accounting in terms of the water phase concentration.

202 *Initial Conditions.* For a steady-state condition the initial conditions don't
 203 matter, but are set to be zero everywhere. For transient simulations in this
 204 work, the steady-state solution is always used as an initial condition.

Table 1: Transport properties and model parameters. To be completed.

205 *2.2.4. Indoor Environment*

206 The indoor air space is modeled as a continuously stirred tank reactor
 207 (CSTR) given by (20). Contaminants are assumed to only enter through the
 208 foundation crack, represented by n_{ck} , which is calculated by integrating the
 209 contaminant flux over the foundation crack boundary. The product of air
 210 exchange rate, which govern how many house volumes are exchanged with
 211 the outside per time unit, and indoor air contaminant concentration gives the
 212 contaminant exit rate. The sorption of contaminant is given by the sorption
 213 reaction term in (22) and the sorbed contaminant concentration is given by
 214 (21).

$$V_{\text{bldg}} \frac{\partial c_{\text{in}}}{\partial t} = n_{ck} - A_e c_{\text{in}} V_{\text{bldg}} + r_{\text{sorb}} V_{\text{mat}} \quad (20)$$

$$V_{\text{mat}} \frac{\partial c_{\text{sorb}}}{\partial t} = -r_{\text{sorb}} V_{\text{mat}} \quad (21)$$

$$r_{\text{sorb}} = k_1 c_{\text{sorb}} - k_2 c_{\text{in}} \quad (22)$$

$$n_{ck} = \int_{A_{ck}} j_{ck} dA \quad (23)$$

215 Here V_{bldg} and V_{mat} are the indoor control volume and volume of indoor
 216 material in m^3 ; c_{in} and c_{sorb} are the indoor and sorbed (onto the indoor
 217 material) contaminant concentrations in mol/m^3 ; n_{entry} is the contaminant
 218 entry rate in mol/s , which is calculated by integrating the contaminant flux
 219 j_{ck} over the foundation crack area; r_{sorb} sorption rate in $\text{mol}/(\text{m}^3 \cdot \text{s})$; k_1 and
 220 k_2 are desorption and sorption reaction constants in $1/\text{s}$.

221 *Fitting Kinetic Parameters.* To calculate the indoor sorption rate we need k_1
 222 and k_2 . These values are found by solving (22) numerically and then finding
 223 the best k_1 and k_2 by fitting them to the experimental data via least square.
 224 We use Runge-Kutta method of order 5(4) as the numerical solve, which
 225 is implemented together with the least square method in the SciPy python
 226 package[15].

227 3. Results & Discussion

228 3.1. Fitting Sorption Parameters

229 Using the numerical fitting scheme described in section 2.2.4 with the
230 sorption data from the method described in section 2.1, the kinetic sorption
231 parameters k_1 and k_2 are determined. Figure 3 shows the result of this fitting
232 and the sorption data for three select materials - wood, Appling soil, and
233 cinderblock concrete. The k_1 and k_2 represent the rate at which TCE desorbs
234 and sorbs respectively onto/from the material of interest. The equilibrium
235 sorption constant is, using the formulation in (22), given by

$$K = \frac{k_1}{k_2} \quad (24)$$

236 and is used as the sorption isotherm. Here a small K indicate that there is
237 a greater propensity for contaminant sorption.

238 To use the soil sorption isotherm in (10) K needs to be converted from be-
239 ing unitless to m^3/kg . This is done by multiplying the inverse of K isotherm
240 with inverse of the soil bulk density ρ_b , which is taken to be $1460 \text{ kg}/\text{m}^3$.

$$K_{\text{ads}} = \frac{1}{K\rho_b} = 5.28 \text{ (m}^3/\text{kg)} \quad (25)$$

241 Table 2 shows the fitted parameters for the tested materials. Based on this
242 these results we can see that cinderblock and soil have orders of magnitude
243 larger sorption capacities than wood or drywall does. We can also see by the
244 k_2 values that soil and cinderblock sorb quickly, much faster than a material
245 with similar sorptive capacity such as paper.

246 *Note: Here I envision some explanation/discussion on why there is a such*
247 *a big difference in sorptive capacities. I've asked Shuai to write about this.*

248 3.2. Soil Sorption's Retarding Effect

Building pressurization is a key factor in VI that influences the advective
contaminant transport. The magnitude of change in response to a pressur-
ization change is significantly influenced by a range of factors, such as soil
permeability, foundation depth, or soil moisture, and of course - sorption,
which we will focus on. To investigate the effect that soil sorption has on
contaminant soil mass transport in the VI context, we run two types tran-
sient simulation where initially the modeled structure is depressurized at a

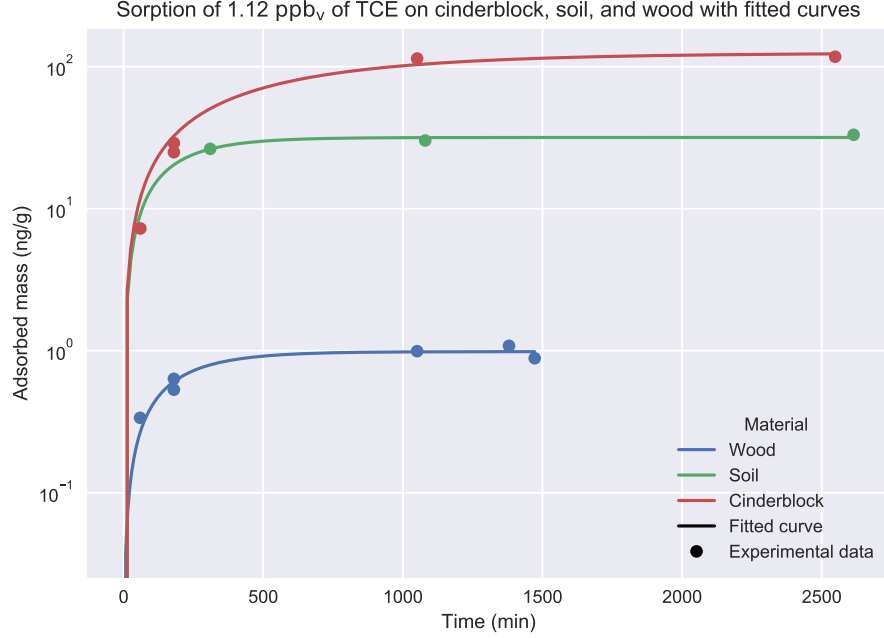


Figure 3: Experimental data of sorption of TCE onto three select materials as well as fitted sorption rates based on the kinetic model (22).

Table 2: Fitted kinetic sorption parameters based on sorption experiment data. Six different types of materials are considered. k_1 and k_2 are the desorption and sorption constants respectively, and K is the sorption equilibrium constant.

Material	k_1 (1/hr)	k_2 (1/hr)	K
Wood	0.32	44.90	$7.10 \cdot 10^{-3}$
Drywall	0.41	87.94	$4.65 \cdot 10^{-3}$
Carpet	0.26	58.74	$4.42 \cdot 10^{-3}$
Paper	0.04	88.37	$4.55 \cdot 10^{-4}$
Soil	0.34	2636.57	$1.30 \cdot 10^{-4}$
Cinderblock	0.10	4175.16	$2.40 \cdot 10^{-5}$

steady -5 Pa. At the start of the simulation, the building building is further depressurized to -15 Pa (26), or overpressurized to 15 Pa (27), and the

simulation is allowed to run for 72 hours.

$$\text{Depressurization : } \Delta p_{\text{in/out}} = \begin{cases} -5, & t = 0 \text{ (hr)} \\ -15, & 0 < t \leq 72 \text{ (hr)} \end{cases} \quad (26)$$

$$\text{Overpressurization : } \Delta p_{\text{in/out}} = \begin{cases} -5, & t = 0 \text{ (hr)} \\ 15, & 0 < t \leq 72 \text{ (hr)} \end{cases} \quad (27)$$

For each of these cases, the simulation is run using two different soil types - sand and sandy loam. Sand is assumed here to not sorb any TCE, while for sandy loam a range of sorption isotherms are used. These range from no sorption ($K_{\text{ads}} = 0 \text{ (m}^3/\text{kg})$) to the experimentally determined sorption isotherm ($K_{\text{ads}} = 5.28 \text{ (m}^3/\text{kg})$) in intervals multiplicative by 10^{-2} . With the experimentally determined isotherm, we see that the ratio between sorbed concentration and soil-gas phase concentration is 7708, i.e. there is a much larger amount of sorbed contaminant. When $K_{\text{ads}} = 5.28 \cdot 10^{-4} \text{ (m}^3/\text{kg})$ this ratio is roughly unity (0.77), which is good to keep in mind in the following discussion. These ranges of values can be used both to represent a soil that has a smaller sorptive capacity or a situation where the sorbed and gas phase has not quite reached equilibrium.

The top panel of Figure 4 shows the indoor air contaminant concentration as the simulated building is undergoing the pressurization in (26) case. Here we can see that for the when the surrounding soil consists of sand, the indoor concentration increases rapidly as the building is further pressurized. The rate of increase decreases significantly for the sandy loam cases, and progressively retards as the sorbed mass increases (K_{ads} increases).

The bottom left panel shows how far away the indoor air concentration (as attenuation factor) for each case is from reaching equilibrium. At the start of the simulation, the building starts with an attenuation of α_0 , which is the steady-state concentration when the building is pressurized with -5 Pa. As the building is further depressurized to -15 Pa, the indoor air concentration will approach a new equilibrium state α_{eq} (the result of which is from a steady-state simulation at that pressurization). By plotting $\frac{|\alpha - \alpha_0|}{|\alpha_{eq} - \alpha_0|}$ we can easily see how far away we are from the new equilibrium state, and a value of 0 represents that we are at the initial concentration, i.e. $\alpha = \alpha_0$, and a value of 1 represents $\alpha = \alpha_{eq}$, i.e. that the new equilibrium has been reached.

This sort of analysis is applied to the bottom right panel as well, but instead of the indoor air concentration (as attenuation factor), we consider

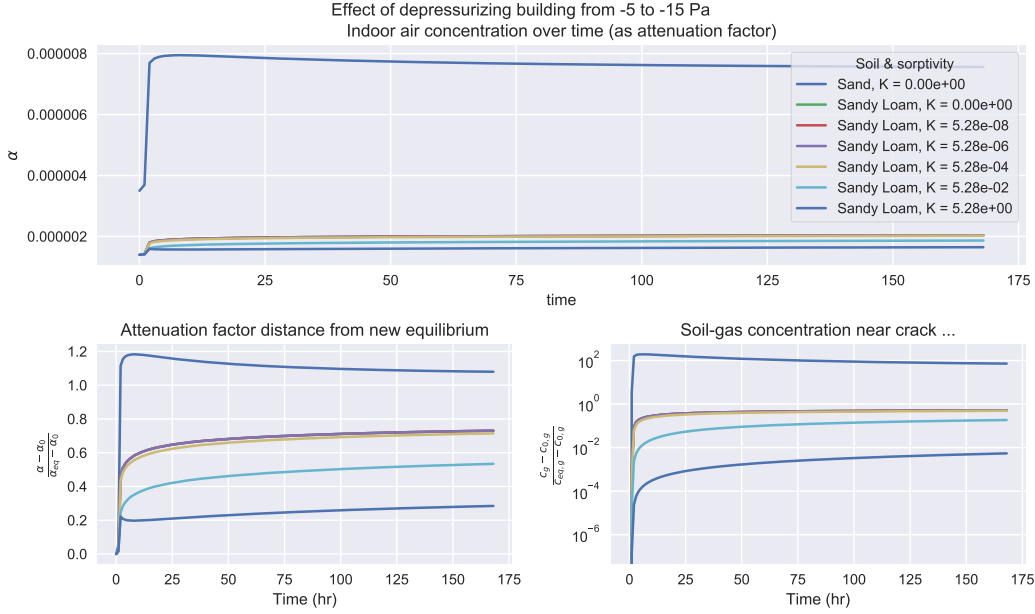


Figure 4

the average soil-gas concentration in a 5 cm diameter cylinder that envelop the entire perimeter crack. The choice of 5 cm is arbitrary, but helps illustrate what happens in the near-foundation-crack region soil-gas concentration, changes in which allow us to better understand how the contaminant is transported into the building from the soil. The same could be done for the soil-gas velocity of course, but the rate of soil-gas velocity change is virtually the same for all of these cases, and reaches the new equilibrium velocity very quickly (much faster than the concentration) and is thus omitted from the figure.

Before discussing the role of sorption here, we can first compare the non-sorbing sand and sandy loam cases. Due to the higher permeability and lower moisture content, sand is significantly more permeable to gas flow than sandy loam (see Table 1 for permeability values). Consequently the advective transport through the foundation crack is much more significant, which is indicated by a Péclet number of around 4 versus 0.2 at a -15 Pa pressurization for sand and sandy loam respectively.

Due to the advection dominated transport mechanism in the sand case, the indoor air concentrations are temporarily elevated above the equilibrium

concentration at -15 Pa, while the soil-gas concentration moves further away from equilibrium. (Note that the absolute distance from equilibrium is plotted in Figure 4 which is why at first glance one might think that the soil-gas concentration is two order of magnitude higher initially, but actually is two order of magnitude lower.) This phenomena occurs because initially more contaminants are drawn into the building from the near crack area than can be resupplied, temporarily depleting the local soil-gas contaminant concentration.

One can notice that many of the sandy loam lines overlap, and start diverging from each other when $K_{\text{ads}} = 5.28 \cdot 10^{-4}$ (m^3/kg), at the point where the ratio of sorbed and soil-gas concentration are roughly equal. We see that this divergence occurs simultaneously in the indoor air and soil-gas contaminant concentration. However, since the indoor air concentration depend on the soil-gas concentration, we know that this is where the relevant difference is.

The simple reason for this is that it is at this threshold the sorptive contribution to the retardation factor (12) starts to becomes larger than the other terms.

$$\rho_b K_H K_{\text{ads}} > \theta_w + \theta_g K_H \quad (28)$$

Thus it is at this point that the contaminant transport in the soil starts to become retarded by sorption. The physical reason for this is that the partitioning between the various phases gives a residence time as the contaminant is transported. Under VI conditions, the values of $\theta_w + \theta_g K_H$ are bounded to relatively small values, while K_{ads} can vary by orders of magnitude, making sorption potentially a very significant retarder for soil transport.

We can also note that the retarding effect of sorption also somewhat depends on the contaminants Henry's Law constant K_H , bulk density ρ_b and the moisture content θ_w . For instance if the ambient temperature is higher, then contaminant K_H is likewise larger, and sorption induced retardation is greater. Generalizing this is difficult however, as K_{ads} is also temperature dependent, and the interplay between these may be complicated. Nevertheless this hints that there may be a climate/weather component to how significantly sorption induced retardation is.

Figure 5 shows the same sort of analysis as in Figure 4 but with the building pressurization following (27). The results here are more or less the same, with the notable exception that in the sand case, the final equilibrium concentration is not initially exceeded. As the building is overpressurized,

the indoor contaminant are pushed out into the soil. Since the indoor air concentration is lower than the soil-gas concentration, this is entirely expected.

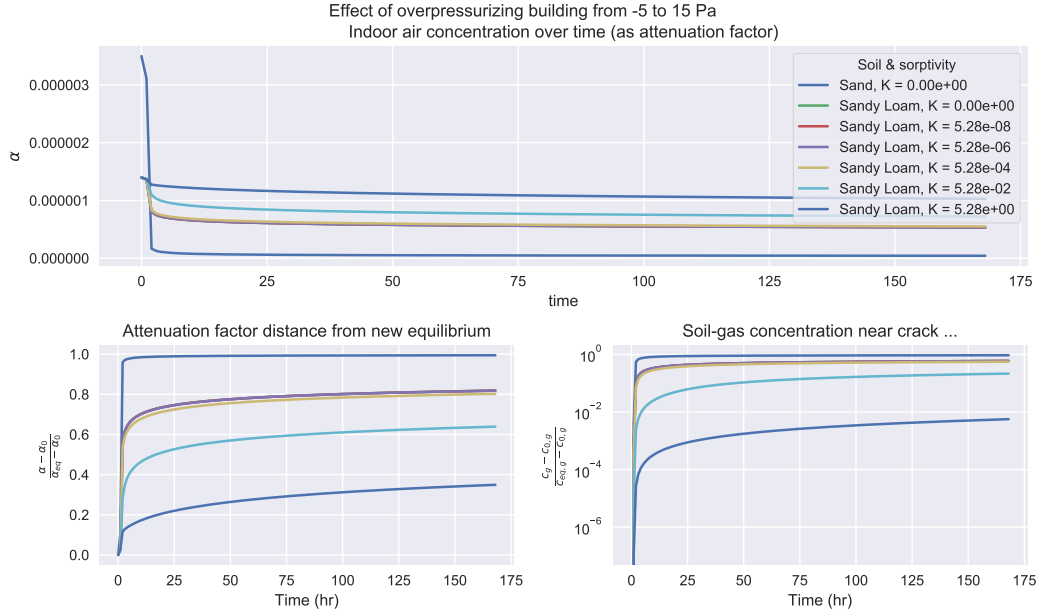


Figure 5

3.3. Indoor Material Sorption And Dynamics

Now we turn to exploring the effect of sorption onto/from various indoor materials has on the indoor air contaminant concentration, again through our model. For these simulations we assume that there is no soil sorption. To study this we consider the basement (the indoor air space) and assume that the inside surfaces are entirely made up of one of the materials we studied in 3.1. We also assume that the material covering the indoor surfaces has a certain thickness or depth that the contaminants can penetrate - giving a certain volume or mass of sorbing material in the indoor. Table 3 shows the surface area, penetration depth, and volume of each material studied. While obviously some of these rooms are non-conventional and arbitrarily designed, i.e. you're unlikely to find a room with carpeted walls, floors, and ceiling, they do present some limiting cases of the potential effect of sorption onto/from these materials.

The modeled building then undergoes a pressurization cycle, where at start of the simulation it is depressurized at -5 Pa and at steady-state. The

Material	d_p (mm)	V_{mat} (m ³)
Cinderblock	5	1.6
Wood	1	0.32
Drywall	10	3.2
Carpet	10	3.2
Paper	0.1	0.032

Table 3: The assumed contaminant penetration depth and subsequent volume of the sorbing indoor materials. The material surface area is assumed to be the same, and each material completely cover the surfaces of a 10x10x3 meter room.

351 building is then sequentially depressurized to -15 Pa, then pressurized to
352 15 Pa, and finally again depressurized to -5 Pa. For each sequence, the
353 new pressurization is maintained for 24 hours. This pressurization cycle
354 may be seen in the top left panel of 6. The choice of pressurization cycle
355 is somewhat arbitrary, but ours can be used to represent limiting cases of
356 natural pressurization variation, or artificially induced pressurization. Figure
357 6 shows the result of these simulations.

358 The change in indoor air contaminant concentration over this pressuriza-
359 tion cycle is shown in the bottom panel of Figure 6. First we consider the
360 reference case - where there is no sorbing indoor materials present. (The
361 blue line is the reference case, which may be difficult to see as the wood and
362 carpet lines overlap.) Here we see that as the building is depressurized, the
363 indoor air contaminant concentration increases quickly in response to the
364 pressurization change, and is approaching an equilibrium.

365 By observation we can see that the presence of the various studied build-
366 ing materials in the indoor environment has a very different effect on the
367 change in indoor air contaminant concentration. The presence of wood and
368 carpet has close to no effect on the indoor air concentration. While cin-
369 derblock has a very significant effect, preventing almost any change in in-
370 door concentration. Drywall and carpet is in the middle significantly delays
371 the rate of change in the indoor concentration, but for each 24 hour cycle,
372 roughly the same indoor concentration is reached as the reference case.

373 The disparity of these result is explained by the the top right panel of
374 Figure 6. Here the de- and sorption rates in $\mu\text{g/hr}$ for each considered indoor
375 material is shown. A positive and negative value here indicate that contami-
376 nant is desorbed respectively sorbed to and from the material. To understand

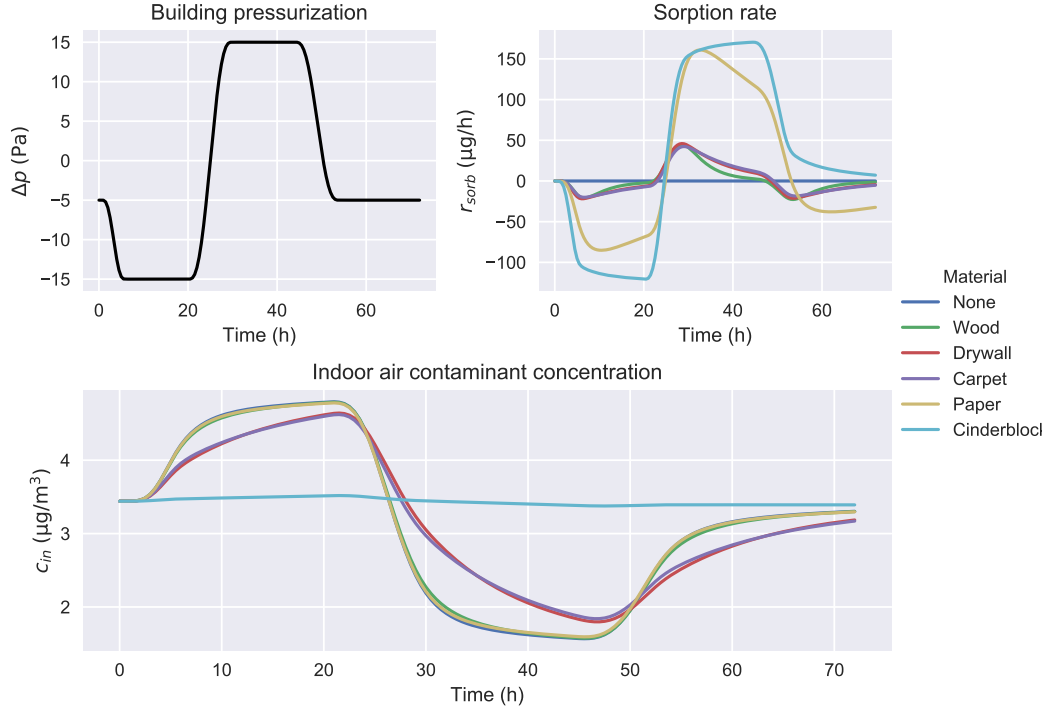


Figure 6: Comparison of how sorption onto/from various indoor materials affect the indoor air contaminant concentration (bottom) of a building that undergoes a pressurization cycle (top left). The rate of de- and sorption for each considered material during the cycle are also shown (top right) and is governed by (22). A positive value means that contaminant vapors are being sorbed onto/into the material and a negative means the material is desorbing into the indoor air space.

377 this figure, it is useful to refer back to Table 2 which show the sorption and
 378 desorption rate constant k_1 and k_2 respectively, and the sorption equilibrium
 379 constant K (a smaller value indicate a larger sorptive capacity).

380 First we consider to the depressurization part of the cycle (1-25 hours).
 381 (Here see that the reference case has no sorption at all, by definition.) And
 382 similar to the indoor concentration panel, we see that the wood, drywall,
 383 and carpet cases overlap. This is explained by these materials have similar
 384 sorptive capacities (K) and sorptive rates (k_2). Paper by contrast has
 385 a similar shape to the three previously mentioned, while the magnitude is
 386 significantly larger. This is because the K value for paper is one order of
 387 magnitude larger, indicating that wood, drywall, and carpet saturate with
 388 contaminant vapors over the time period, while paper does not. Cinderblock

389 has a further order of magnitude larger K value, thus is even further away
390 from being saturated, which explains the even faster sorption rate.

391 Next we consider the overpressurization period (25-49 hours). Again we
392 see here that wood, drywall, and carpet behave the similarly for the same
393 reasons as before, i.e. the desorption rate constants k_1 and sorption equilib-
394 rium constants K are similar. This means that these reach the new sorbed
395 contaminant saturation at roughly the same time.

396 Here it is important to note that due to the diffusion dominated transport
397 through the foundation crack, even though the building is overpressurized,
398 there is substantial contaminant entry. And because the sole contaminant
399 source is the modeled contaminated groundwater, the sorbed equilibrium is
400 relative to this entry rate.

401 Paper and cinderblock initially behave very similarly during the overpres-
402 surization period and desorb contaminants quickly. However, paper reaches
403 its saturation limit after a relatively short time, while cinderblock has not
404 even at the end of the overpressurization cycle. Since the desorption rate
405 constants k_2 are relatively similar for the materials, thus this disparity is
406 primarily due to the different sorption equilibrium constants K .

407 Lastly, we consider the final period where the pressurization goes back
408 to its initial state (49-72 hrs). Here we see that the reference case does
409 not quite return to the initial indoor concentration. Thus the contaminant
410 entry rate has not equilibrated yet, due to the soil contaminant concentration
411 has not done so either. Like in the previous analysis we again see that
412 the wood, drywall, and carpet cases don't differ from the reference. The
413 paper case is slightly more different, but for the same reasons that have
414 already been discussed. Cinderblock is unique here though, as we clearly see
415 that it is releasing contaminants, due to the previous change in contaminant
416 concentration has been so significantly retarded.

417 From this simulation work we can see how varied the effect of sorbing
418 indoor materials are. Most of the tested materials only have a moderate effect
419 on the indoor air contaminant concentration dynamics, with the notable
420 exception of cinderblock, which effectively enforces a pseudo-steady-state.
421 However we also see from the analysis of the sorption dynamics that the de-
422 and sorption rate constants k_1 and k_2 are less important than the sorptive
423 capacity K of the material.

424 3.4. Indoor Material Sorption And Mitigation

425 The work done by us and others have shown the large sorptive capacities
426 of various common materials. The desorption of the sorbed contaminants
427 may have significant impact on the efficacy of various mitigation systems. To
428 investigate this we turn to our model and consider a scenario where initially
429 the modeled building is depressurized with -5 Pa and at the start of the
430 simulation some perfect mitigation scheme is turned on and the contaminant
431 entry n_{entry} in (20) goes to zero. We also assume that for each case, the indoor
432 environment contains the same amount of indoor material as described in
433 section 3.3. The air exchange rate is assumed to remain a constant 0.5 per
434 hour for the entire 72 hour simulation time.

435 The decrease in indoor air concentration (as attenuation factor α) for each
436 simulated case is seen in Figure 7. As expected, when there is no sorbing
437 indoor materials, i.e. our reference case, the indoor concentration decreases
438 log-linearly. We can also see that the contaminant desorption from the
439 materials maintain a higher indoor air concentration relative to reference,
440 with cinderblock again shown to have the great impact.

441 *Note that this section is still incomplete as I am still working on expand-*
442 *ing/improving the analysis/figure.*

443 4. Conclusions

444 Acknowledgements

445 This project was supported by grant ES-201502 from the Strategic Envi-
446 ronmental Research and Development Program and Environmental Security
447 Technology Certification Program (SERDP-ESTCP).

448 Declaration of interest: none

449 References

- 450 [1] R. Meininghaus, L. Gunnarsen, H. N. Knudsen, Diffusion and Sorp-
451 tion of Volatile Organic Compounds in Building Materials-Impact on
452 Indoor Air Quality, Environ. Sci. Technol. 34 (15) (2000) 3101–3108.
453 doi:10.1021/es991291i.
- 454 [2] R. Meininghaus, E. Uhde, Diffusion studies of VOC mixtures in a build-
455 ing material, Indoor Air 12 (4) (2002) 215–222. doi:10.1034/j.1600-
456 0668.2002.01131.x.

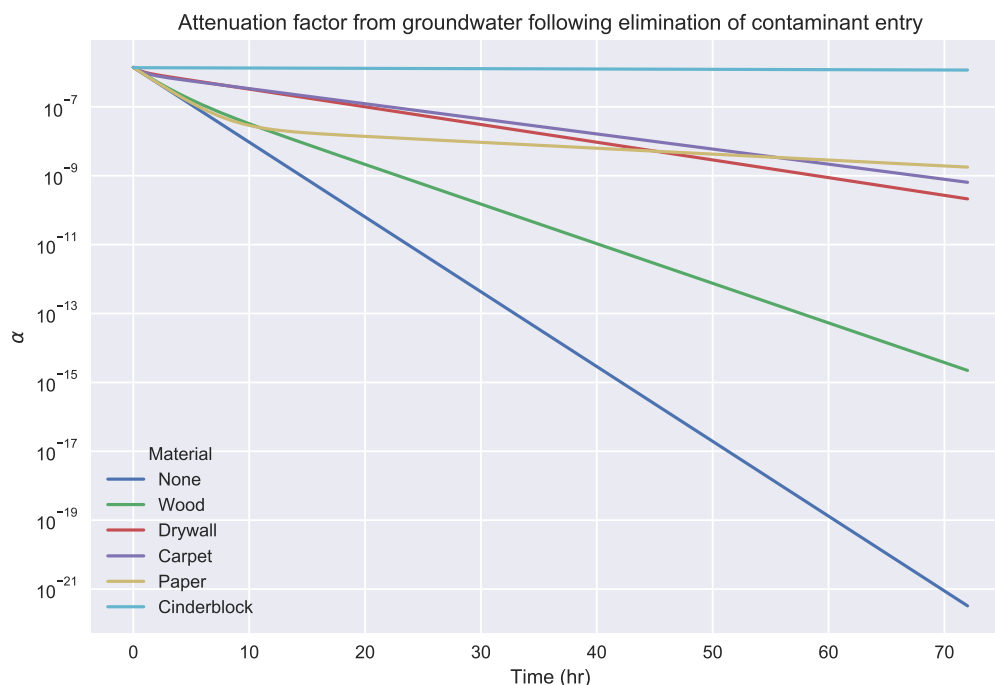


Figure 7

- 457 [3] F. D. Tillman, J. W. Weaver, Review of Recent Research on Vapor
458 Intrusion (2005) 47.
- 459 [4] X. Wang, Y. Zhang, J. Xiong, Correlation between the solid/air
460 partition coefficient and liquid molar volume for VOCs in build-
461 ing materials, Atmospheric Environment 42 (33) (2008) 7768–7774.
462 doi:10.1016/j.atmosenv.2008.05.030.
- 463 [5] J. Xu, J. S. Zhang, X. Liu, Z. Gao, Determination of partition and
464 diffusion coefficients of formaldehyde in selected building materials and
465 impact of relative humidity, J. Air Waste Manag. Assoc. 62 (6) (2012)
466 671–679. doi:10.1080/10962247.2012.665812.
- 467 [6] A. Bodalal, J. S. Zhang, E. G. Plett, A method for measuring internal
468 diffusion and equilibrium partition coefficients of volatile organic com-
469 pounds for building materials, Building and Environment 35 (2) (2000)
470 101–110. doi:10.1016/S0360-1323(99)00005-0.

- 471 [7] U.S. Environmental Protection Agency, OSWER Technical Guide for
472 Assessing and Mitigating the Vapor Intrusion Pathway From Subsurface
473 Vapor Sources To Indoor Air (2015).
- 474 [8] C. Holton, Y. Guo, H. Luo, P. Dahlen, K. Gorder, E. Dettenmaier,
475 P. C. Johnson, Long-Term Evaluation of the Controlled Pressure Method
476 for Assessment of the Vapor Intrusion Pathway, *Environ. Sci. Technol.*
477 49 (4) (2015) 2091–2098. doi:10/f64j45.
- 478 [9] C. C. Lutes, R. S. Truesdale, B. W. Cosky, J. H. Zimmerman,
479 B. A. Schumacher, Comparing Vapor Intrusion Mitigation System
480 Performance for VOCs and Radon, *Remediation* 25 (4) (2015) 7–26.
481 doi:10/gd6dfn.
- 482 [10] U.S. Environmental Protection Agency, Assessment of Mitigation Sys-
483 tems on Vapor Intrusion: Temporal Trends, Attenuation Factors, and
484 Contaminant Migration Routes under Mitigated And Non-mitigated
485 Conditions (2015).
- 486 [11] T. McHugh, P. Loll, B. Eklund, Recent advances in vapor intrusion
487 site investigations, *Journal of Environmental Management* 204 (2017)
488 783–792. doi:10/gd6dgk.
- 489 [12] R. Shen, K. G. Pennell, E. M. Suuberg, A numerical investigation of
490 vapor intrusion — The dynamic response of contaminant vapors to
491 rainfall events, *Science of The Total Environment* 437 (2012) 110–120.
492 doi:10/f4fp9s.
- 493 [13] J. G. V. Ström, Y. Guo, Y. Yao, E. M. Suuberg, Factors affect-
494 ing temporal variations in vapor intrusion-induced indoor air contam-
495 inant concentrations, *Building and Environment* 161 (2019) 106196.
496 doi:10.1016/j.buildenv.2019.106196.
- 497 [14] M. T. van Genuchten, A Closed-form Equation for Predicting the Hy-
498 draulic Conductivity of Unsaturated Soils, *Soil Sci. Soc. Am.* 44 (5)
499 (1980) 892–898. doi:10/fdc8mc.
- 500 [15] E. Jones, T. Oliphant, Pearu Peterson, SciPy: Open source scientific
501 tools for Python (2011).